Table 3. *A summary of transmission reactions producing only DSC residues*

We give fourteen different reaction groups, each exhibiting different numbers of available reactions of various types. The coincidence systems belonging to the reaction groups are also listed below the group descriptions, with the appropriate values of c^2/a^2 given in parentheses.

Reaction type	Number of possible reactions
(*a*) Reaction group 1	
Perfect → perfect	18
Perfect → partial	0
Partial → perfect	0
Partial → partial	2
Total	20

($\frac{12}{5}$): $\Sigma 9$, $\Sigma 21a$, $\Sigma 21b$, $\Sigma 27$, $\Sigma 33$, $\Sigma 39a$, $\Sigma 39b$; ($\frac{33}{13}$): $\Sigma 24$; ($\frac{51}{20}$): $\Sigma 37$; ($\frac{18}{7}$): $\Sigma 13$, $\Sigma 17$, $\Sigma 23a$, $\Sigma 29$, $\Sigma 31$, $\Sigma 35a$, $\Sigma 35b$, $\Sigma 43$, $\Sigma 47$, $\Sigma 49a$, $\Sigma 49b$; ($\frac{21}{8}$): $\Sigma 15b$, $\Sigma 39$; ($\frac{27}{10}$): $\Sigma 19$, $\Sigma 23$, $\Sigma 33b$; ($\frac{27}{8}$): $\Sigma 17$, $\Sigma 27a$, $\Sigma 41a$, $\Sigma 45b$; ($\frac{39}{11}$): $\Sigma 24$.

(*b*) Reaction group 2	
Perfect → perfect	18
Perfect → partial	6
Partial → perfect	6
Partial → partial	2
Total	32

($\frac{12}{5}$): $\Sigma 12$, $\Sigma 24$, $\Sigma 36$, $\Sigma 48$.

(*c*) Reaction group 3	
Perfect → perfect	18
Perfect → partial	6
Partial → perfect	6
Partial → partial	594
Total	624

($\frac{12}{5}$): $\Sigma 16$, $\Sigma 32$, $\Sigma 44$.

transmission of lattice partial dislocations in h.c.p. crystals, although, for certain values of $(c/a)^2$, $\Sigma = 2N$ and $\Sigma = 3N$ cases may fall into some particular reaction group, as illustrated by the results presented in Table 3.

As for the case of dislocation absorption, transmission or transformation reactions involving one or more lattice partials with site-switching Burgers vectors always produce PDSC dislocations in the grain-boundary plane.

This work was supported by the National Science Foundation, under grant No. DMR-8601433.

References

BACMANN, J.-J., SILVESTRE, G., PETIT, M. & BOLLMANN, W. (1981). *Philos. Mag. A*, **43**, 189-200.

BLERIS, G. L., NOUET, G., HAGEGE, S. & DELAVIGNETTE, P. (1982). *Acta Cryst.* A**38**, 550-557.

BOLLMANN, W. (1970). *Crystal Defects and Crystalline Interfaces.* Berlin: Springer.

BOLLMANN, W., MICHAUT, B. & SAINFORT, G. (1972). *Phys. Status Solidi A*, **13**, 637-649.

BONNET, R., COUSINEAU, E. & WARRINGTON, D. H. (1981). *Acta Cryst.* A**37**, 184-189.

BROKMAN, A. (1981). *Acta Cryst.* A**37**, 500-506.

CHEN, F.-R. (1986). PhD Thesis, State Univ. of New York at Stony Brook.

CHEN, F.-R. & KING, A. H. (1984). *Mater. Sci. Eng.* **66**, L25-L26.

CLARK, W. A. T. & SMITH, D. A. (1978). *Philos. Mag. A*, **38**, 367-385.

FUKUTOMI, H., KAMIJO, T. & HORIUCHI, R. (1986). *Grain Boundary Structure and Related Phenomena: Proc. JIMIS-4.* Supplement to *Trans. Jpn Inst. Met.* pp. 929-936.

GRIMMER, H. & WARRINGTON, D. H. (1987). *Acta Cryst.* A**43**, 232-243.

HIRTH, J. P. & BALLUFFI, R. W. (1973). *Acta. Metall.* **21**, 929-942.

KING, A. H. (1982). *Acta Metall.* **30**, 419-427.

KING, A. H. & CHEN, F.-R. (1984). *Mater. Sci. Eng.* **66**, 227-237.

KING, A. H. & SMITH, D. A. (1980). *Acta Cryst.* A**36**, 335-343.

POND, R. C. & SMITH, D. A. (1977). *Philos. Mag.* **36**, 353-366.

SMITH, D. A. (1980). *Scr. Metall.* **14**, 715-718.

SMITH, D. A. & POND, R. C. (1976). *Int. Metall. Rev.* **21**, 61-74.

SUN, C. P. & BALLUFFI, R. W. (1982). *Philos. Mag. A*, **46**, 49-62.

SUTTON, A. P. (1984). *Int. Metall. Rev.* **29**, 377-402.

Acta Cryst. (1987). B**43**, 422-429

$(Ni,Mg)_{4n+6}Ge_{2n+1}O_{8(n+1)}$, a New Structural Family Related to Olivine and Spinel

BY JACQUES BARBIER

Department of Geology, University of Western Ontario, London, Ontario N6A 5B7, Canada

(*Received* 4 *March* 1987; *accepted* 11 *May* 1987)

Abstract

A new structural family, $(Ni,Mg)_{4n+6}Ge_{2n+1}O_{8(n+1)}$ ($n = 1, 2, 3, 4, \infty$), has been identified at atmospheric pressure in the NiO-MgO-GeO_2 system. Its building principle is based on regular intergrowth of n (001) olivine layers (*Pnma* setting) with one {111} cation-deficient rock-salt layer. Alternatively, individual structures are shown to contain spinel elements, the proportion of which decreases with increasing values of n. This new family therefore provides a structural transition between the olivine ($n = \infty$ end-member) and spinel structure types and may be relevant to the high-pressure olivine → spinel transformation.

1. Introduction

During the course of a re-investigation of the NiO-MgO-GeO_2 system at atmospheric pressure, a new

0108-7681/87/050422-08$01.50

compound, $(Ni,Mg)_{10}Ge_3O_{16}$, has recently been identified and characterized by powder X-ray and electron diffraction (Barbier, 1987). Its crystal structure has been described as a 3:1 intergrowth of {111} layers of the spinel and rock-salt structures or, alternatively, as a 1:1 intergrowth of (001) olivine layers (for the *Pnma* setting of the olivine unit cell) and {111} layers of a cation-deficient rock-salt structure (*cf.* Fig. 3*a*).

The latter description shows that the $(Ni,Mg)_{10}Ge_3O_{16}$ structure is very simply related to that of $Mg_{14}Ge_5O_{24}$ determined earlier by Von Dreele, Bless, Kostiner & Hughes (1970) and corresponding to a 2:1 intergrowth of olivine layers and cation-deficient rock-salt layers. This structural relationship suggests the existence of an homologous series based on a variable ratio of olivine (ol) and rock-salt (d) layers with the general formula:

$$M_{4n+6}Ge_{2n+1}O_{8(n+1)} = n\,M_4Ge_2O_8\,(\text{ol}) + M_6GeO_8\,(\text{d})$$

where the members $n = 1$ and $n = 2$ correspond to the $(Ni,Mg)_{10}Ge_3O_{16}$ and $Mg_{14}Ge_5O_{24}$ structures respectively.

The present paper describes the building principle of this structural family and reports observations by high-resolution electron microscopy (HREM) of some of its members co-existing in the NiO–MgO–GeO_2 system at atmospheric pressure.

2. Description of the $(Ni,Mg)_{4n+6}Ge_{2n+1}O_{8(n+1)}$ family

2.1. *Building principle: relation to the olivine structure*

The crystal structure of $Mg_{14}Ge_5O_{24}$ (Von Dreele *et al.*, 1970) is shown in Fig. 1 projected on (010) (for the *Pcma* setting of the *Pbam* space group): as described by the original authors, the O atoms form a mixed cubic-hexagonal (hc^2) close-packed array with metal atoms in octahedral (Mg and Ge) and tetrahedral (Ge) coordination. Along the z direction, double olivine layers (ol) with the stoichiometry $2\,Mg_4Ge_2O_8$ alternate with single cation-deficient rock-salt layers (d) with the stoichiometry Mg_6GeO_8. Accordingly, the strucure can be formally described by the equation:

$$Mg_{14}Ge_5O_{24} = 2\,Mg_4Ge_2O_8\,(\text{ol}) + Mg_6GeO_8\,(\text{d}).$$

[Note that Mg_2GeO_4 itself crystallizes with the olivine structure at normal pressure and temperatures above 1083 K (Dachille & Roy, 1960).]

For comparison, the olivine structure of α-Co_2SiO_4 (Morimoto, Tokonami, Watanabe & Koto, 1974) is depicted in Fig. 2 in the equivalent projection: the relation to the $Mg_{14}Ge_5O_{24}$ structure is obvious.

The $M_{4n+6}Ge_{2n+1}O_{8(n+1)}$ (M = metal atom) structural family is simply generated from the $Mg_{14}Ge_5O_{24}$ structure by altering the number n of olivine layers intergrown with a single rock-salt layer. The resulting structures are shown in Fig. 3 (idealized to perfect oxygen close-packing) for the values of $n = 1, 2, 3$ and 4. One end-member of the series is obviously olivine itself, M_2GeO_4 ($n = \infty$), and the other end-member is $M_{10}Ge_3O_{16}$ ($n = 1$) rather than M_6GeO_8 ($n = 0$) as the latter structure would not contain any olivine layer. [It is noteworthy, however, that the member $n = 0$ corresponds to the structure of the mineral murdochite, Cu_6PbO_8 (Christ & Clark, 1955).] Although structures with $n < 1$ (*i.e.* with more rock-salt layers than olivine layers) are geometrically feasible, none has been identified in this study of the NiO–MgO–GeO_2 system (*cf.* below), and the $M_{4n+6}Ge_{2n+1}O_{8(n+1)}$ series seems to be restricted to $n \geq 1$.

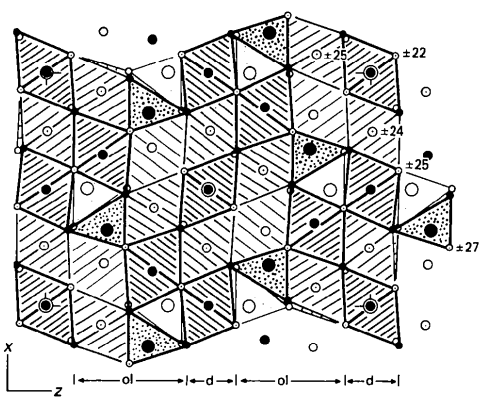

Fig. 1. The $Mg_{14}Ge_5O_{24}$ structure (Von Dreele *et al.*, 1970) projected on (010) (*Pcma* setting) consisting of double olivine layers (ol) alternating, in the z direction, with single cation-deficient rock-salt layers (d). Large, medium and small circles are Ge, Mg and O atoms respectively. Open, filled and dotted circles are at heights 0, 50 and ~±25 (in units of $b/100$). Note that some Ge atoms are octahedrally coordinated within the d layers.

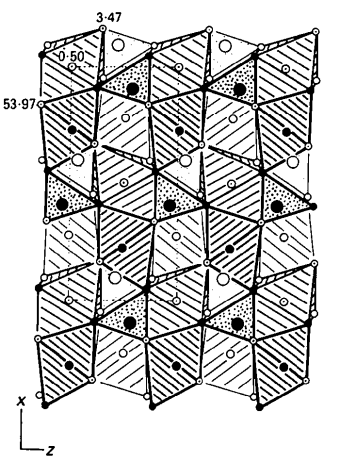

Fig. 2. The olivine-type structure of α-Co_2SiO_4 (Morimoto *et al.*, 1974) projected on (010) (*Pnma* setting). Large, medium and small circles are Si, Co and O atoms respectively. Open, filled and dotted circles are at heights 25, 75 and ≃0, 50 (in units of $b/100$). Note the simple relation to the $Mg_{14}Ge_5O_{24}$ structure (Fig. 1) and the greater distortion of the oxygen packing in the olivine structure.

As seen in Fig. 3, the close-packed oxygen array changes progressively across the $M_{4n+6}Ge_{2n+1}O_{8(n+1)}$ series: from cubic c for $n=1$, to mixed cubic-hexagonal hc^2, h^2c^2 and h^3c^2 for $n=2$, 3 and 4 respectively, to hexagonal h for $n=\infty$ (olivine). The nth member of the series therefore corresponds to the stacking sequence c^2h^{n-1} of oxygen layers with orthorhombic and monoclinic unit cells for even and odd values of n respectively. Assuming a perfect close-packing of O atoms with a shortest O···O distance of 2·98 Å, ideal cell parameters can be calculated for any member of the series: they are listed in Table 1 for the structures corresponding to $n=1, 2, 3$ and 4. A good agreement is found with the experimental data available for phases in the NiO–MgO–GeO_2 system (Table 1), taking into account that the cell dimensions of a particular structure type decrease with increasing Ni/Ni+Mg ratio (*cf.* Ringwood, 1961; Navrotsky, 1973).

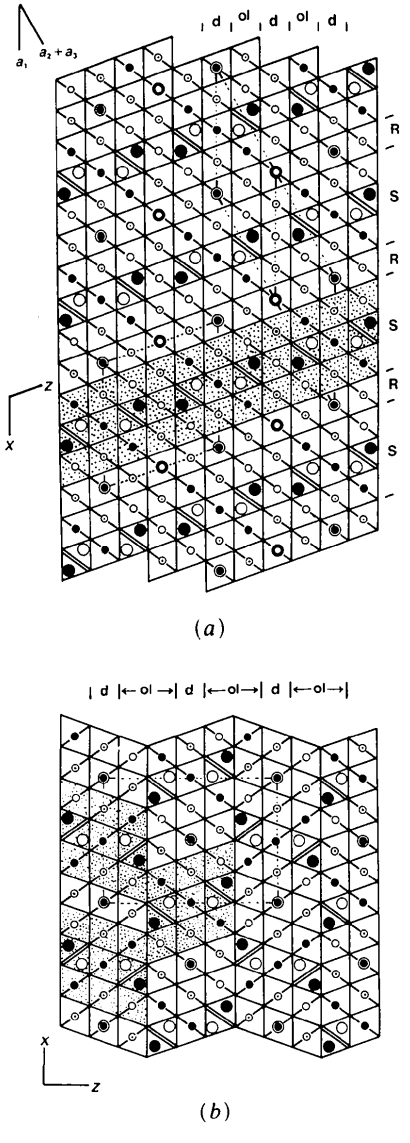

Fig. 3. Schematic drawings of the (010) projections of the ideal structures of the $M_{4n+6}Ge_{2n+1}O_{8(n+1)}$ series: (*a*) $M1$ ($n=1$), (*b*) $M2$ ($n=2$), (*c*) $M3$ ($n=3$), and (*d*) $M4$ ($n=4$). A monoclinic pseudocell and the true rhombohedral cell have both been outlined for the $M1$ structure (*cf.* Barbier, 1987). Large and small circles are Ge and (Ni,Mg) atoms respectively, O atoms have been omitted. Open, filled and dotted circles are at heights 0, 50 and ±25 (in units of $b/100$). Olivine (ol) and rock-salt (d) layers have been indicated. Spinel blocks (3×3 octahedra in $M2$, $M3$ and $M4$) and slabs (in $M1$) are stippled. Compare with Fig. 4.

2.2. *Relation to the spinel structure*

As described elsewhere (Barbier, 1987), the $(Ni,Mg)_{10}Ge_3O_{16}$ structure is also simply related to spinel: it consists of an intergrowth of three {111} spinel layers with one {111} rock-salt layer, stacked along the [111] direction of the rhombohedral unit cell (*cf.* Fig. 3*a*). [For comparison, the spinel structure of γ-Fe_2SiO_4 (Marumo, Isobe & Akimoto, 1977) is shown in Fig. 4.] The spinel slabs (S) and rock-salt

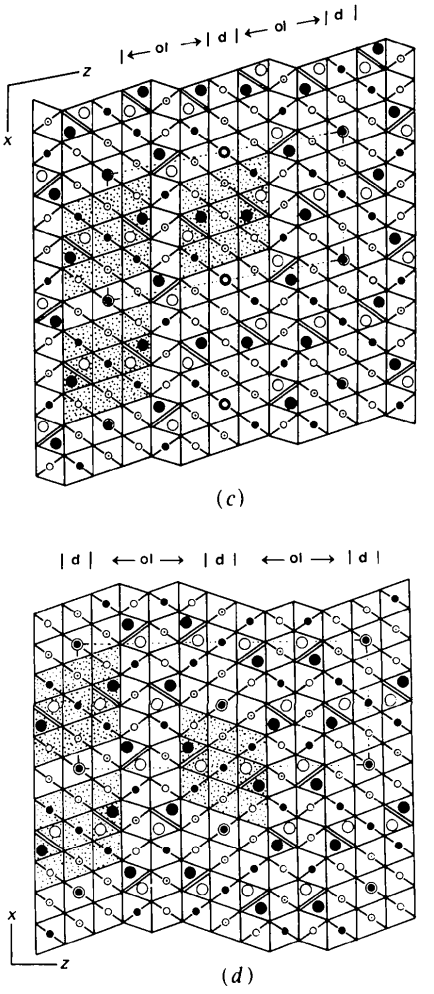

Fig. 3 (*cont.*)

layers (R) in Fig. 3(*a*) have the stoichiometries $M_7Ge_2O_{12}$ and M_3GeO_4 respectively, so that formally, $M_{10}Ge_3O_{16} = M_7Ge_2O_{12}$ (spinel) + M_3GeO_4 (rock salt). [Note that in the present description, the rock-salt layers are stoichiometric, unlike the cation-deficient d layers in the previous description based on olivine.]

Spinel elements are also readily recognized in the crystal structures of the other members of the $M_{4n+6}Ge_{2n+1}O_{8(n+1)}$ series (Figs. 3*b–d*). However, the spinel slabs S present in the $M_{10}Ge_3O_{16}$ structure are now broken up into blocks (3×3 octahedra in size) intergrown with smaller rock-salt blocks (3×1 octahedra in size) and olivine-type layers (for $n \geq 3$). As n increases, the proportion of spinel blocks decreases while that of olivine layers increases so that the $M_{4n+6}Ge_{2n+1}O_{8(n+1)}$ series represents a transition between spinel-like and olivine-like structures.

The compound $(Ni,Mg)_{10}Ge_3O_{16}$ has been observed experimentally to be unstable at high temperature (at normal pressure) and to decompose according to the reaction (Barbier, 1987):

$$3(Ni,Mg)_{10}Ge_3O_{16} \rightarrow (Ni,Mg)_{22}Ge_9O_{40} + 8(Ni,Mg)O$$
$$(n=1) \qquad (n=4)$$

Based on the above descriptions of the crystal structures in terms of spinel and olivine elements, this decomposition reaction is equivalent to the well-known high-temperature spinel → olivine transformation occurring, for instance, in Mg_2GeO_4 (Dachille & Roy, 1960).

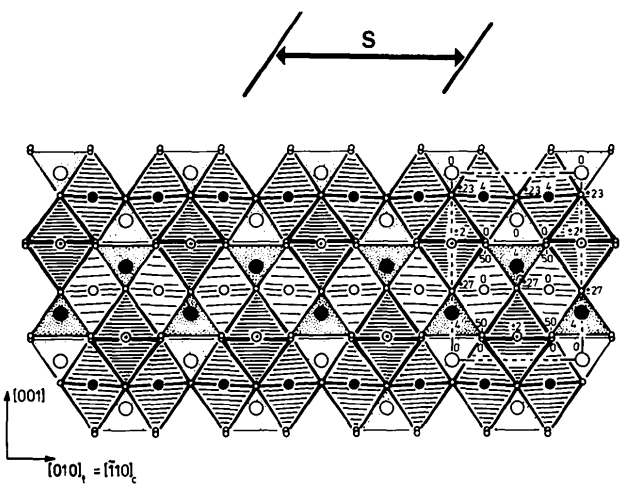

Fig. 4. The spinel structure of γ-Fe_2SiO_4 (Marumo *et al.*, 1977) projected on $(100)_t = (110)_c$. [The subscripts *c* and *t* refer to the conventional face-centred cubic unit cell and to the smaller body-centred tetragonal cell related to *c* by the matrix $(\frac{1}{2}\frac{1}{2}0/-\frac{1}{2}\frac{1}{2}0/001)$.] Large, medium and small circles are Si, Fe and O atoms respectively. Heights of metal atoms are expressed in 1/8 of the a_t repeat and those of O atoms in 1/100. One slab (S) identical to those in Fig. 3(*a*) has been indicated.

3. Observations of $M_{4n+6}Ge_{2n+1}O_{8(n+1)}$ phases in the NiO–MgO–GeO_2 system

Most of the observations reported here have been made on samples synthesized during the investigation of the $(Ni,Mg)_{10}Ge_3O_{16}$ phase (Barbier, 1987) without attempting to determine detailed phase relations in the NiO–MgO–GeO_2 system.

Polycrystalline samples were prepared by high-temperature sintering of high-purity (99·99%) NiO, MgO and GeO_2 powders. The final heat treatment consisted in a heating period of two days at 1673 K in a sealed platinum capsule (to prevent loss of GeO_2 by evaporation) followed by an air quench. Most products were multiphase assemblages and, as expected from the cell parameters in Table 1, a severe overlapping of lines occurred in the powder X-ray diffraction patterns. Accordingly, electron diffraction combined with high-resolution electron microscopy (HREM) proved to be the most suitable technique for phase identification. For this purpose, finely crushed grains were deposited on a holey carbon film supported by a copper grid, and were examined with a Hitachi 800 electron microscope operating at 200 kV and equipped with a tilt-rotation side-entry specimen holder. [A few higher-resolution images (Figs. 8 and 12) have been recorded with a JEOL 200CX electron microscope.]

Some preliminary single-crystal-growth experiments were also performed using a flux technique (PbO flux, slow cooling at 2–4 K h^{-1} from 1573 to 1173 K). Sizeable crystals were obtained for the phases *M*1 ($n=1$), *M*2 ($n=2$) and $(Ni,Mg)_2GeO_4$ olivine ($n=\infty$) (the *M*1 crystals, however, being invariably multiply twinned).

A schematic phase diagram for the (Ni,Mg)O-rich region of the NiO–MgO–GeO_2 system is shown in Fig. 5. It is based on earlier data published by Ringwood (1961) and Navrotsky (1973) but has been modified in order to include the *M*1 phase,

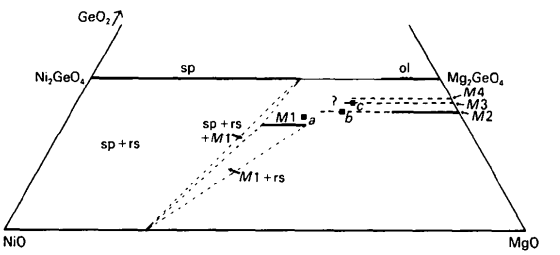

Fig. 5. Schematic phase diagram for the NiO–Ni_2GeO_4–Mg_2GeO_4–MgO system at atmospheric pressure and 1673 K showing the locations of the $(Ni,Mg)_{4n+6}Ge_{2n+1}O_{8(n+1)}$ phases for n = 1–4. Abbreviations sp, ol and rs denote spinel, olivine and rock-salt phases. Heavy lines correspond to 'solid solution' ranges: data for the Ni_2GeO_4–Mg_2GeO_2 join are from Ringwood (1961) and data on the NiO–MgO join are from Navrotsky (1973). Dashed lines indicate undetermined composition ranges and phase boundaries. Points *a*, *b* and *c* represent bulk compositions used for the observations by electron microscopy.

$(Ni_xMg_{1-x})_{10}Ge_3O_{16}$ [$x \simeq 0{\cdot}4$–$0{\cdot}5$ (Barbier, 1987)], as well as the proposed $M2$, $M3$ and $M4$ phases. The composition range indicated for the $M2$ phase has been derived from electron microprobe analysis of two flux-grown single crystals, giving an atomic ratio $Mg/Ni \simeq 4{\cdot}8$. [As indicated in Fig. 5, this range possibly extends toward higher Ni contents.] No data have been obtained concerning the composition ranges of the $M3$ and $M4$ phases due to the lack of single-phase products and to unsuccessful attempts to grow single crystals.

The samples investigated by electron diffraction/microscopy correspond to the three bulk compositions marked *a*, *b* and *c* in the phase diagram of Fig. 5 and to the reaction products from the high-temperature decomposition of the $M1$ phase. As noted earlier, these samples were multiphase assemblages often consisting, on a microscopic scale, of complex intergrowths of various phases of the $M_{4n+6}Ge_{2n+1}O_{8(n+1)}$ series. However, single-phase grains of the $M1$, $M2$ and $M4$ phases were not uncommon and Fig. 6 shows the corresponding electron diffraction patterns recorded along equivalent directions, *i.e.* $[10\bar{1}0]_{M1} \| [010]_{M2,M4}$ [for the hexagonal unit cell of the $M1$ phase; note also the orientation relationship $(01\bar{1}2)_{M1} \| (001)_{M2,M4}$ which is consistent with the structure models of Fig. 3]. The strong 006 ($M2$) and 0010 ($M4$) reflections show the six- and ten-layer character of the corresponding structures and the relations $d_{100}(M2) = d_{100}(M4)$ and $d_{024}(M1) = d_{006}(M2) = d_{0010}(M4)$ are consistent with the cell parameters listed in Table 1. [Note that, in the $M1$ pattern, the (hkl, $-h+k+l \neq 3n$) reflections are absent as expected from the rhombohedral symmetry, whereas in the $M2$ and $M4$ patterns, the forbidden reflections of the *Pcma* space group, *i.e.* ($hk0$, $h \neq 2n$) and ($0kl$, $l \neq 2n$), appear *via* multiple diffraction.]

As expected from the phase diagram, the sample with bulk composition *a* gave a mixture of the $M1$ and $M2$ phases mainly. They often formed disordered intergrowths as shown in Fig. 7: $M1$ slabs of various widths, characterized by the 110° monoclinic cell angle and the 9·5 Å spacing ($= d_{003}$ rhombohedral cell or d_{100} monoclinic cell), occur in an $M2$ matrix with a *c* repeat of 14·4 Å. All phase boundaries are parallel to (001) planes which is again consistent with the structure models in Fig. 3. Note the presence of several $M3$-type faults in the left-hand part of Fig. 7 corresponding to a *c* repeat of ~19 Å. Another faulted $M2$ grain from the same sample is shown in Fig. 8 containing a narrow slab (about 120 Å wide) of the $M3$ phase.

Products from the bulk compositions *b* and *c* contained mixtures of the $M2$ and $M4$ phases along with small amounts of the $M3$ phase. Figs. 9 and 10 show

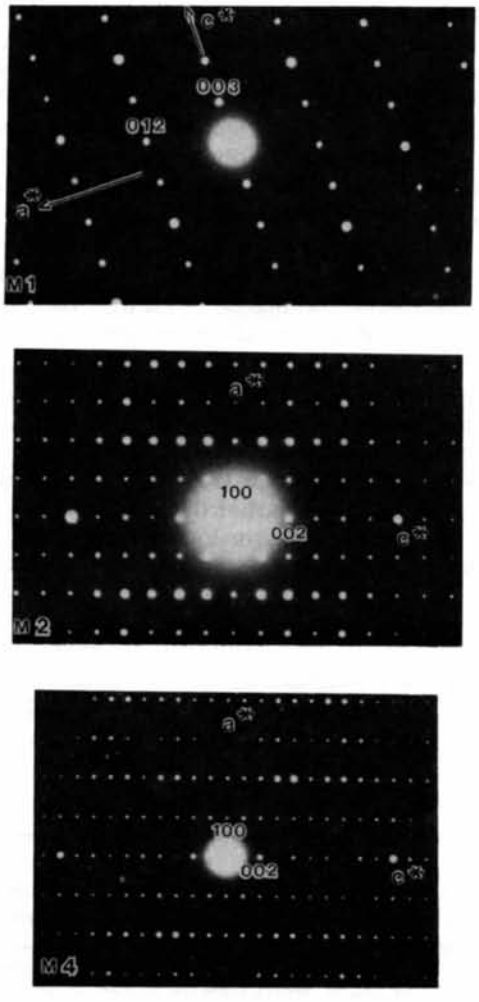

Fig. 6. Electron diffraction patterns recorded from single-phase $M1$, $M2$ and $M4$ grains along equivalent crystallographic directions, *i.e.* $[10\bar{1}0]_{M1}$ (hexagonal indexing) and $[010]_{M2,M4}$ (*cf.* Fig. 3).

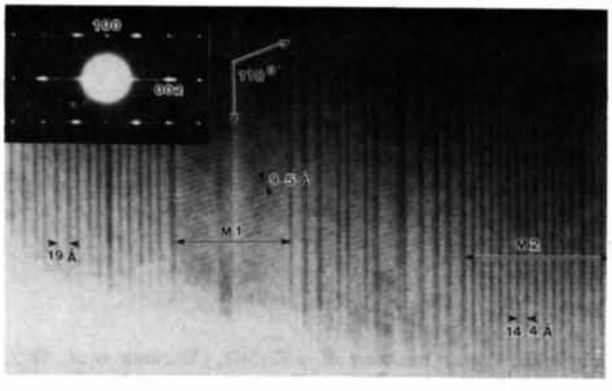

Fig. 7. Disordered intergrowth of the $M1$ and $M2$ phases observed in a sample with bulk composition *a* in Fig. 5. The indices in the diffraction pattern refer to the $M2$ unit cell. Intergrowth takes place on (001) planes as expected from the structural models. Note several $M3$-type faults with a *c* repeat of 19 Å.

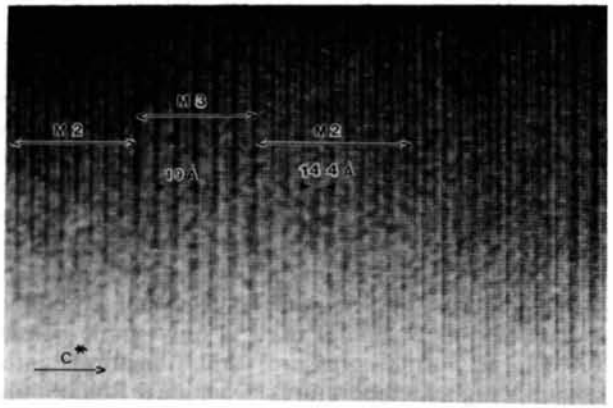

Fig. 8. Tilted image of a faulted $M2$ grain containing a narrow slab (about 120 Å wide) of the $M3$ phase. The latter was only observed as faults or thin slabs of this kind in all the samples examined.

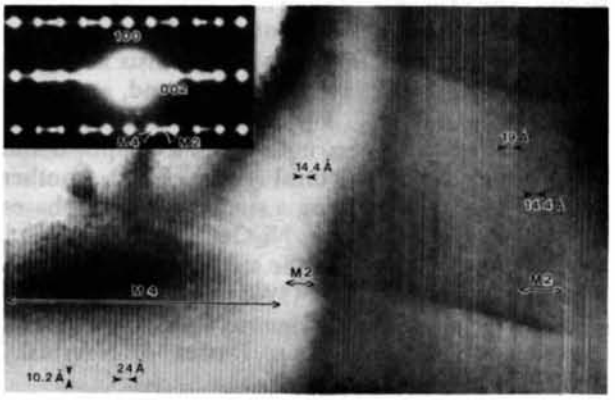

Fig. 9. [010] Zone-axis image of a grain containing $M4$ as the major phase (*cf.* diffraction pattern) along with a small amount of the $M2$ phase. Several 19 Å faults are also visible.

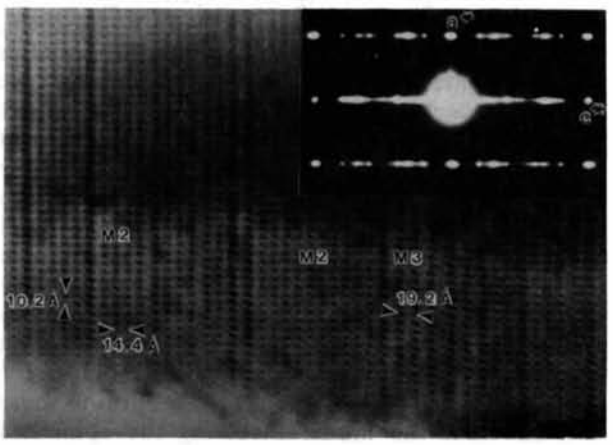

Fig. 10. Faulted $M2$ grain from a sample with bulk composition *b* in Fig. 5. The monoclinic symmetry of the $M3$ slab is clearly visible with a measured angle of about 96°.

Table 1. *Cell parameters for some* $(Ni,Mg)_{4n+6}Ge_{2n+1}O_{8(n+1)}$ *phases*

Ideal cell parameters, calculated for a perfect close-packing of G atoms with a shortest O···O distance of 2·98 Å, are given in parentheses.

Compound	a(Å)	b(Å)	c(Å)	β(°)	Reference
$Ni_4Mg_6Ge_3O_{16}$*	10·121	5·886	10·201	109·6	Barbier (1987)
	(10·32)	(5·96)	(10·32)	(109·47)	
$Mg_{14}Ge_5O_{24}$†	10·219	5·944	14·512		Von Dreele
	(10·32)	(5·96)	(14·60)		*et al.* (1970)
$(Ni_{0·17}Mg_{0·83})_{14}Ge_5O_{24}$‡	10·18	5·92	14·43		This work
$(Ni,Mg)_{22}Ge_9O_{40}$	10·162	5·914	24·091		This work
	(10·32)	(5·96)	(24·33)		
$(Ni,Mg)_{18}Ge_7O_{32}$	(10·32)	(5·96)	(19·76)	(100·0)	
Mg_2GeO_4 olivine	10·295	6·030	4·915		Navrotsky (1973)
	(10·32)	(5·96)	(4·87)		

* Parameters for the monoclinic pseudocell. The true cell is rhombohedral with the hexagonal parameters $a = 5·887$ and $c = 28·603$ Å (Barbier, 1987).
† For the *Pcma* setting of the original *Pbam* space group.
‡ Precession film data from a flux-grown single crystal.

[010] zone-axis images of typical grains consisting of single- and multiphase regions. It is noteworthy that, whereas single-phase $M2$ and $M4$ grains were commonly encountered, the $M3$ phase was only observed as a minor component occurring as faults or thin slabs. The measurement of the monoclinic angle of the $M3$ unit cell in Fig. 10 gives an approximate value of 96° not too different from the ideal angle of 100° listed in Table 1.

It has been mentioned earlier that the $M1$ phase decomposes at high temperature into a mixture of $M4$ and rock-salt phases. [The cell parameters listed in Table 1 for the $(Ni,Mg)_{22}Ge_9O_{40}$ phase have actually been refined from powder X-ray data obtained from this decomposition product.] HREM observations, however, revealed the presence of small amounts of $M2$ and $M3$ phases intergrown within the $M4$ grains (Fig. 11) as well as trace amounts of olivine (Fig. 12). Comparison of the high-resolution image of the $M4$ phase in Fig. 12 with the drawing of its crystal structure in Fig. 3(*d*) indicates that the

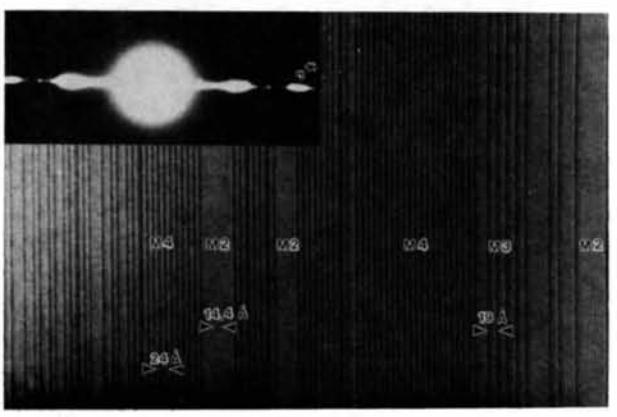

Fig. 11. Disordered intergrowth of the $M4$, $M2$ and $M3$ phases resulting from the high-temperature decomposition of the $M1$ phase.

double rows of white dots in the image can be associated with the rock-salt d layers, alternating in the z direction with four-layer-thick olivine slabs.

4. Discussion

The present experimental observations confirm the existence of a new structural family, $(Ni,Mg)_{4n+6}Ge_{2n+1}O_{8(n+1)}$. At least three of its members, $M1$ ($n=1$), $M2$ ($n=2$) and olivine ($n=\infty$) are stable phases at atmospheric pressure as indicated by the successful growth of single crystals. The $M4$ phase may be stable at high temperature only as suggested by the observation of large single-phase grains in the products quenched from 1873 K but the failure to obtain single crystals using a flux-growth technique over the temperature interval 1573–1173 K. The presence of olivine in the high-temperature products (*cf.* Fig. 12) also suggests that the $M4$ phase may decompose into a mixture of olivine plus rock salt at still higher temperatures. Finally, the $M3$ phase is perhaps metastable as it could only be identified as small amounts intergrown with other members of the series.

$Mg_{14}Ge_5O_{24}$ is the only phase of the $M_{4n+6}Ge_{2n+1}O_{8(n+1)}$ family to have been reported in the nickel-free MgO–GeO_2 system. It had been wrongly identified as Mg_4GeO_6 in the phase diagram published by Robbins & Levin (1959) (the true stoichiometry being determined later by Von Dreele *et al.*, 1970) who also reported that it decomposes directly into a mixture of $MgO + Mg_2GeO_4$ olivine at about 1768 K. In view of the present results for the NiO–MgO–GeO_2 system, it seems likely that this decomposition involves in fact extra intermediate phases such as the $M4$ phase, *i.e.*, $Mg_{22}Ge_9O_{40}$. On the other hand, the existence of the $M1$ phase ($Mg_{10}Ge_3O_{16}$) in the MgO–GeO_2 system might be restricted to low temperatures because of the high proportion of spinel elements in its crystal structure: indeed, Mg_2GeO_4 spinel itself is only stable below 1083 K (at normal pressure) and transforms into olivine at higher temperatures (Dachille & Roy, 1960).

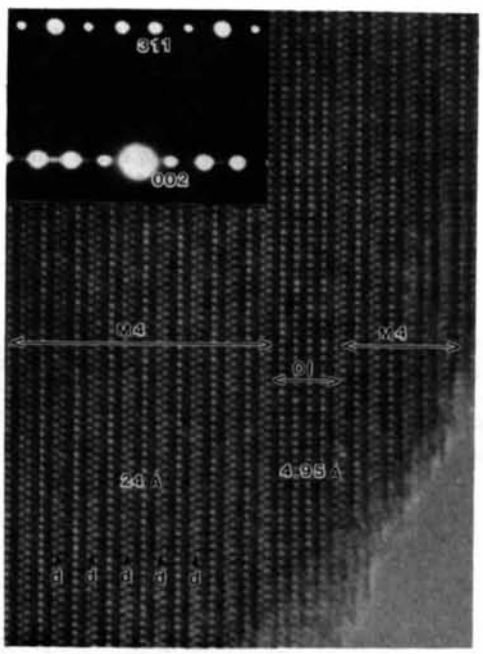

Fig. 12. High-resolution image of an $M4$ grain observed in the decomposition products of the $M1$ phase at high temperature. A narrow slab with the olivine structure is intergrown within the grain. Comparison with the structure model in Fig. 3(d) allows the double rows of white dots to be associated with the rock-salt d layers alternating with olivine slabs.

A structural family similar (if not identical) to the $M_{4n+6}Ge_{2n+1}O_{8(n+1)}$ series probably exists in the CoO–MgO–GeO_2 system, as Navrotsky (1973) reported several unidentified phases corresponding to a molar fraction $X_{GeO_2} \simeq 0{\cdot}24$ (*cf.* $X_{GeO_2} = 0{\cdot}23$, $0{\cdot}26$ and $0{\cdot}29$ for the phases $M1$, $M2$ and $M4$ respectively). The existence of such a series in the Co system would only reinforce the similarity with the Ni system: in both cases, a two-phase gap exists along the spinel–olivine join (Navrotsky, 1973) and, as seen in Fig. 5, the $M_{4n+6}Ge_{2n+1}O_{8(n+1)}$ series could be regarded as filling in this gap, not only in a compositional sense but also in a structural sense (*cf.* § 2). Another system possibly containing a similar series of phases is FeO–MgO–GeO_2: like Ni_2GeO_4 and Co_2GeO_4, Fe_2GeO_4 crystallizes with the spinel structure at normal pressure [*e.g.* Wyckoff (1965)] and the FeO–MgO join consists also in a continuous solid solution with the rock-salt structure [*e.g.* Davies & Navrotsky (1983)].

The smooth structural transition between the olivine and spinel structure types provided by the $M_{4n+6}Ge_{2n+1}O_{8(n+1)}$ series may be relevant to the olivine → spinel high-pressure transformation. Just as the spinelloid phases observed in the $NiAl_2O_4$–Ni_2SiO_4 and $MgGa_2O_4$–Mg_2GeO_2 systems (Ma, 1974; Akaogi, Akimoto, Horioka, Takahashi & Horiuchi, 1982; Barbier & Hyde, 1986) have been proposed as possible intermediates in a martensitic-type olivine ⇄ spinel transition (Hyde, White, O'Keeffe & Johnson, 1982; Madon & Poirier, 1983), the present series could provide an alternative path for the same transformation. It would, however, correspond to a nucleation and growth mechanism as the diffusion of atomic species (*i.e.* cations) would be required in order to accommodate the different stoichiometries of the various M_n phases. Such a transformation would lead to the following olivine/spinel orientation relationships: $(001)_{ol} \| (\bar{1}11)_{sp}$ and $[010]_{ol} \| [110]_{sp}$ (*cf.* Figs. 2 and 3). These relations are identical to those derived from the model involving the spinelloid family [*e.g.* Hyde *et al.* (1982)] and are also consistent with experimental observations [*e.g.* Hamaya & Akimoto (1982), Boland & Liu (1983)]. It is also

interesting to note that the $M_{4n+6}Ge_{2n+1}O_{8(n+1)}$ series is intermediate between olivine and spinel in terms of density of atom packing: in the $MgO-GeO_2$ system, the structures of Mg_2GeO_4 spinel, $Mg_{14}Ge_5O_{24}$ and Mg_2GeO_4 olivine correspond to volumes of 17·58, 18·36 and 19·04 Å^3 per O atom respectively [values based on data from Von Dreele *et al.* (1970) and Navrotsky (1973)].

Because germanates are usually regarded as lower-pressure analogues of silicates (*e.g.* Ringwood, 1975), the existence of the $(Ni,Mg)_{4n+6}Ge_{2n+1}O_{8(n+1)}$ series at atmospheric pressure suggests that a similar structural family may exist at high pressure in silicate systems such as $MgO-SiO_2$. In that respect, it is interesting to point out that in their investigation by electron microscopy of the olivine → spinel transition in Mg_2SiO_4, Boland & Liu (1983) observed olivine crystals heavily faulted on (001) planes (for the *Pnma* setting of the olivine unit cell). Although these faults, observed at low magnification, have been associated with the olivine → Ω-phase transition [the Ω-phase being the 'linking' spinelloid phase – *cf.* Hyde *et al.* (1982)], the same type of faults would also be expected from disordered (001) intergrowths of thin slabs of phases from the $Mg_{4n+6}Si_{2n+1}O_{8(n+1)}$ series (*cf.* Figs. 7–11). It appears that high-resolution electron microscopy would be required in order to distinguish between, in particular, images of thin slabs of the two linking $M1$ and Ω structures: both correspond to a cubic close-packing of O atoms but, whereas the Ω-phase contains olivine-type layers only (Hyde *et al.*, 1982), the $M1$ phase is a 1 : 1 intergrowth of olivine and rock-salt layers. The only difference between the two structures therefore resides in the cation content and distribution within half of the cubic close-packed layers. Finally, it may be noted that the cation distribution in the structures of the hypothetical $Mg_{4n+6}Si_{2n+1}O_{8(n+1)}$ series would require some Si atoms to be six-coordinated within the d rock-salt layers. Although this condition suggests that these structures could only be stable at relatively high pressures, it may not be prohibitive as very high pressures are indeed involved in these transformations [*e.g.* 220 kbar (22 GPa) in Boland & Liu's experiment].

References

AKAOGI, M., AKIMOTO, S. HORIOKA, S., TAKAHASHI, K. & HORIUCHI, H. (1982). *J. Solid State Chem.* **44**, 257–267.

BARBIER, J. (1987). *J. Solid State Chem.* **67**, 52–60.

BARBIER, J. & HYDE, B. G. (1986). *Phys. Chem. Miner.* **13**, 382–392.

BOLAND, J. N. & LIU, L. G. (1983). *Nature (London)*, **303**, 233–235.

CHRIST, C. L. & CLARK, J. R. (1955). *Am. Mineral.* **40**, 907–916.

DACHILLE, F. & ROY, R. (1960). *Am. J. Sci.* **258**, 225–246.

DAVIES, P. K. & NAVROTSKY, A. (1983). *J. Solid State Chem.* **46**, 1–22.

HAMAYA, N. & AKIMOTO, S. (1982). *Phys. Earth Planet. Inter.* **29**, 6–11.

HYDE, B. G., WHITE, T. J., O'KEEFFE, M. & JOHNSON, A. W. S. (1982). *Z. Kristallogr.* **160**, 53–62.

MA, C. B. (1974). *Contrib. Mineral. Petrol.* **45**, 257–279.

MADON, M. & POIRIER, J. P. (1983). *Phys. Earth Planet. Inter.* **33**, 31–44.

MARUMO, F., ISOBE, M. & AKIMOTO, S. (1977). *Acta Cryst.* B**33**, 713–716.

MORIMOTO, N., TOKONAMI, M., WATANABE, M. & KOTO, K. (1974). *Am. Mineral.* **59**, 475–485.

NAVROTSKY, A. (1973). *J. Solid State Chem.* **6**, 21–41.

ROBBINS, C. R. & LEVIN, E. M. (1959). *Am. J. Sci.* **257**, 63–70.

RINGWOOD, A. E. (1961). *Aust. J. Sci.* pp. 378–379.

RINGWOOD, A. E. (1975). In *Composition and Petrology of the Earth's Mantle*. New York: McGraw-Hill.

VON DREELE, R. B., BLESS, P. W., KOSTINER, E. & HUGHES, R. E. (1970). *J. Solid State Chem.* **2**, 612–618.

WYCKOFF, R. W. G. (1965). In *Crystal Structures*, 2nd ed. New York: Interscience.

Acta Cryst. (1987). B**43**, 429–434

$K_x(Nb,W)_{17}O_{47}$ ($1 \le x \le 2$): a New Tunnel Structure Derived from High-Resolution Electron Micrographs

BY MARGARETA SUNDBERG AND MONICA LUNDBERG

Department of Inorganic Chemistry, Arrhenius Laboratory, University of Stockholm, S-106 91 Stockholm, Sweden

(*Received* 19 *January* 1987; *accepted* 18 *May* 1987)

Abstract

A new tunnel structure of a fully oxidized compound with the general formula $K_xNb_{8+x}W_{9-x}O_{47}$ ($1 \le x \le 2$) has been deduced from high-resolution electron micrographs. For $x = 2$ the monoclinic unit-cell parameters are $a = 18{\cdot}882\,(5)$, $b = 3{\cdot}9572\,(5)$, $c = 12{\cdot}378\,(2)$ Å, $\beta = 102{\cdot}93\,(3)°$, $V = 901{\cdot}41$ Å^3, $Z = 1$, $M_r = 3046{\cdot}2$ and $D_x = 5{\cdot}61$ g cm^{-3}. The space group is $P2/m$. The structure has been confirmed by simulated image calculations and by X-ray powder diffraction studies. The polyhedral framework is built up of octahedra and pentagonal columns in such a way that four-, five- and six-sided tunnels are formed. The structure comprises features of both the $W_{18}O_{49}$ and the tetragonal tungsten bronze (TTB) structure types.

0108-7681/87/050429-06$01.50